The Buoyancy Reynolds Number Instability and Thermohaline Staircase Formation in the Polar Oceans

Yuchen Ma and W.R.Peltier

University of Toronto, 60 St.George Street, Toronto, Canada

(Dated: May 4, 2022)

Abstract

The Arctic Ocean main thermocline may be characterized by a series of fine-scale thermohaline staircase structures that are present in a wide range of regions, the formation mechanism of which remains unclear. Recent analysis has led to the proposal of a theoretical model which suggested that these staircase structures form spontaneously in the salinity and temperature-stratified ocean when the turbulent intensity determined by the buoyancy Reynolds number Re_b is sufficiently weak ([1]). In the current work, we have designed a series of Re_b controlled direct numerical simulations of turbulence in the Arctic Ocean thermocline to test the effectiveness of this theory. In these simulations, the staircases form naturally when Re_b falls in the range predicted by the instability criterion that is the basis of the proposed theory. In the DNS analyses described we show that the exponential growth-rate of the layering mode of instability matches well with the prediction of [1]. The staircases formed in our simulations are further compared with the classical diffusive interface model initially proposed by [2], which argued that stable staircase structures can only form when the density ratio R_ρ is smaller than the critical value of $R_\rho^{cr} = \tau^{-1/2}$. Here τ is the ratio of haline diffusivity over thermal diffusivity. We show that the staircase structures can stably persist in the model regardless of whether or not $R_\rho < R_\rho^{cr}$ is satisfied because of the involvement of stratified turbulence in the interfaces of the staircase.

INTRODUCTION

Thermohaline staircases are a strikingly organized structures in the oceans which are characterized by a series of vertically well mixed layers of both heat and salt separated by sharp interfaces (see chapter 8 of [3] for a recent review). Depending on whether the relatively warmer and saltier waters are lying above or below the relatively colder and fresher waters, the thermohaline staircases can be classified into salt-fingering staircases which are usually observed in low and mid latitude oceans and the diffusive-convection staircases which are mainly observed in the polar oceans. The first observations of these two types of thermohaline staircases were reported in the late 1960s ([4], [5]) and their origins were quickly connected with the two types of double-diffusive convection: salt-fingering and diffusive-convection. However, half a century later, we are only "half-way" towards a complete understanding of their formation mechanisms: while we have already gained the ground-breaking understanding of the detailed mechanism for the salt-fingering staircases,

its still unclear what the key mechanism is that is responsible for the formation of the diffusive-convection staircases.

On the salt-fingering side of the story, the formation of the staircase structures has been understood through the instability of the flux-gradient laws that are characteristic of doubly diffusive mixing. The critical theory for layer formation in this circumstance has been discussed in the work of [6], which has been referred to as the γ instability theory in the literature on staircase formation. In this work, the author assumed that the large scale effect of the stochastic field of salt fingers can be described by parametrized effective diapycnal diffusivities for heat K_Θ and salt K_S which are determined solely on the density ratio $R_\rho^{SF} \equiv \Theta_z/S_z$ (here Θ and S are the potential temperature field and salinity, both in density units). Following from this assumption, the author analyzed the linear stability of the parametrized mean field model and derived the criterion on basis of which the system will be susceptible to a layering instability if the parametrized flux ratio $\gamma^{SF} \equiv R_\rho^{SF} K_\Theta/K_S$ is a decreasing function of R_ρ^{SF}. The dependence of K_Θ and K_S on R_ρ^{SF} was calibrated using a series of direct numerical simulations (DNSs) (e.g. [7],[8], [9] and [10]), field measurements (e.g. [11]) and the theoretical modeling (e.g. [12], [9]). All above contributions establish the existence of a clear trend of decreasing γ^{SF} with increasing R_ρ^{SF} when R_ρ^{SF} is small. Meanwhile, accumulating evidences has established that spontaneous formation of salt-fingering staircases from the mechanism of [6] which includes direct numerical simulations (e.g. [13]), basin-scale model simulation (e.g. [14]), mean-field model simulations (e.g. [15], [16], [17]). Most importantly, the multi-scale version of the flux-gradient model proposed by [16] successfully solved the ultraviolet catastrophe problem that existed in the original theoretical framework of [6]. The growth-rate of the instability in this new model is shown to decrease to a very small value after R_ρ reaches the value of 1.8, which perfectly explains why nearly all the salt-fingering staircases observed in the ocean have the density ratio R_ρ^{SF} smaller than 2 (see [18] or [3] for a review).

The above explanation for salt-fingering staircase formation suggests that the salt-fingering fluxes formed from salt-fingering instability and resulting turbulence alone are sufficient to drive the system into a layered state. However, this simple picture does not suffice to provide an explanation of staircase formation in the diffusive-convection regime. While most diffusive-convection staircases have been found to exist in a large range of density ratio $2 < R_\rho < 9$ (see [19], [20] for example), (here $R_\rho \equiv S_z/\Theta_z$ is the density ratio for

the diffusive convection system), the linear diffusive-convection instability is only active in a tiny window of the parameter space $1 < R_\rho < 1.16$ (see [3]). This strongly suggests that the linear diffusive- convection regime can not be regarded as the ultimate cause of the formation of diffusive-convection staircases, for example, that are observed in the Arctic Ocean. Therefore, it is the common belief for researchers in this field that another missing piece of information has to be introduced in the diffusive-convection circumstance to solve this problem. One of the most promising candidates for the explanation has been that associated with thermohaline-shear instability theory initially proposed by [21] and in this case this missing piece of information is "shear". In this work and the following work of [22], [23], it is demonstrated that a flow that is stable to both shear instability and diffusive-convection instability might become unstable under the joint action of diffusive-convection and different forms of shear. It has been further shown that these instabilities are able to develop into layered structures in the non-linear evolution of direct numerical simulations ([21]). While the thermohaline-shear instability perfectly solves the problem of the mismatch between the different ranges of density ratio, the development for the instability is still currently dependent on some specific form of the shear (e.g., a vertically sinusoidal form is considered [21] and the time-dependent form is considered in [22], [23]). Another candidate explanation for the diffusive-convection staircases is the thermohaline intrusion mechanism discussed by [24] and [25] where the missing piece of information is imagined to be the "horizontal gradient". This theory was firstly discussed to explain the formation of salt-fingering staircases in [24] and it has been extended to explain the diffusive-convection staircases by [25]. While the coexistence of thermohaline intrusion and double-diffusive staircases are often apparent in the observational data as shown in [25], it remains a challenging question as to whether the presence of horizontal gradients is a necessary condition for staircases to form in the diffusive-convection regime, considering that salt-fingering staircases have now been shown to be able to form without horizontal gradients in the γ instability theory of [6].

While these two candidate theories described above may significantly contribute to our understanding of the problem, we believe that there should exist a theory for the formation of diffusive convection staircases which is as straightforward and instability-based as that which has been shown to apply in the salt fingering case. Recently, such a new theory for the formation of layering in the diffusive convection regime was proposed in [1] (hereafter referred to as MP21). In this paper a formation mechanism is illustrated using the same

mean field framework for the instability analysis of flux-gradient laws as in the previous work of [6], namely that involving the effective turbulent diapycnal diffusivities for heat K_Θ and salt K_S which are parametrized to represent the average transport properties of the micro-scale fluid dynamics. However, in the work of MP21 K_Θ and K_S are parametrized as depend only upon the non-dimensional parameter referred to as the buoyancy Reynolds number $Re_b = \epsilon/(\nu N^2)$ (here ν is the kinematic viscosity, ϵ is the viscous dissipation rate and $N = \sqrt{-g/\rho_0 \langle d\overline{\rho}/dz \rangle}$ is the BruntVisl frequency) instead of the density ratio which plays the critical role in the formation of salt fingering staircases. The hypothesis that underlies this different choice of governing non-dimensional parameter is that the formation of the diffusive-convection staircases originates from the background stratified turbulence itself instead of diffusive convection instability. One mechanism that leads to layer formation from stratified turbulence is that previously proposed by [26] and further discussed most recently by [27], but their analyses apply only to a fluid in which density is determined by only a single advecting and diffusing species. Since Arctic Ocean staircases involve perfectly correlated steps in both temperature and salinity it is clear that no analysis based upon the assumption of a single component fluid can suffice the solution of the problem. Nevertheless, and as explicitly discussed in MP21, the Phillips mechanism for the staircase in the salinity component of Arctic staircases is lurking in the background of the results for the two-component system. The proposal in MP21 is the first detailed demonstration of how a thermohaline staircase could emerge directly out of turbulence in a two-component fluid in which the background stratification is in the diffusive convection regime. By analyzing the linear stability of the parametrized mean field model that is based on the local buoyancy Reynolds number and assumes the specific functional dependence of $K_\Theta(Re_b)$ and $K_S(Re_b)$ described by [28], MP21 demonstrated that the a system defined by constant background gradient in both temperature and salinity will be susceptible to a layering mode of instability if the buoyancy Reynolds number satisfies the criterion for instability. For this reason, we will refer to the theory described in MP21 as the Re_b instability theory in what follows for simplicity.

There are two lines of evidence that strongly support the Re_b instability theory as a highly plausible mechanism for the formation of staircase structures in the diffusive convection environment of the Arctic Ocean. First, the mean-field model simulation performed in MP21 confirmed that the initially fastest growing mode follows the Re_b instability mechanism and

does grow into the layered state in the non-linear stage of evolution. Second, the criterion in MP21 which states that whether layers will form or do not is determined by the turbulence level determined by Re_b and independent of R_ρ is consistent with a series of oceanographic measurements (e.g. [20], [29]), as discussed in details in MP21.

Despite these supporting evidences there remain two critical questions upon which we will focus in the present paper. First, we will test whether development of the Re_b instability will inevitably lead to the formation of a thermohaline staircase structure in a DNS of a three dimensional fully developed turbulent flow. It needs to be kept in mind that the current form of Re_b instability theory describe in MP21 is a linear stability theory that relies on a series of idealized assumptions, and therefore it is crucial for us to evaluate its effectiveness using that resolve the smallest scales of fluid dynamics. Second, we want to understand whether the thermohaline staircase state formed from the Re_b instability will remain as a stable structures after they first form and what mechanism is responsible for keeping such interfaces stable. In the early literature a comprehensive theoretical analysis of the diffusive interfaces that separate distinct steps in a staircase was developed by [2], hereafter LS. The model developed in this work has kept been used as the basis for the analyses on the diffusive interface structure by researchers in this field (e.g. [30] , [31]). An important prediction of LSs theory is that no steady interface structure can exist when $R_\rho > \tau^{-1/2}$ ($\tau = \kappa_s/\kappa_\theta$ is the ratio of molecular diffusivities for salt and heat, $\tau^{-1/2} \approx 10$ in the Arctic Ocean), whereas the Re_b instability theory predicts that the system is unstable to the layering mode at any R_ρ that is larger than 1. Therefore, the second major goal of this paper is to explore the range of the stably staircase structure formed in our DNSs and compare it with the classical theory of LS. It should be noticed that although most of the diffusive-interfaces have been found in regions with $R_\rho < 10$ in the measurements of ocean and lakes (and this has always been regarded as criterion for diffusive-interfaces, see review of [32] for example), observed diffusive staircases with $R_\rho > 10$ do exist occasionally (e.g. [33], [34]).

In the process of addressing the primary goals of this paper, we will conduct a series of DNSs designed to address the questions raised in the above paragraph. In these series of simulations, we consider the homogeneous system consisting of a fluid in which density is determined by two diffusing species driven by the stochastic forcing of large-scale vortical modes. Vortical mode body-forcing has been implemented in previous work to study homogenous stratified turbulence (e.g. [35], [36], [37], [38]). It is well suited for the exploration

of layer formation occurring through Re_b instability since it allows us to properly control the energy input into the system that is required to control the averaged Re_b of the system. As we will demonstrate in what follows, if and only if the average buoyancy Reynolds number lies in the unstable regime predicted by MP21 will the system develop into a layered state.

The remainder of the paper will be arranged as follows. In section 2 we will give a brief review of the derivation of the Re_b instability theory. The settings of the DNSs employed in this work will be presented in section 3. In the following section 4 we will describe the time evolution of the system and illustrate how the layered structure forms in the system. These simulation results will be analyzed and compared with the theoretical prediction of MP21 in various different ways. In section 5 we will analyze the interface structure formed in our numerical system in details to illustrate how the stable staircase state is maintained and compare it with the classical theory of LS. Finally we summarize our conclusions in section 6.

SUMMARY OF Re_b INSTABILITY THEORY

In this section, we will briefly review the original formulation of the Re_b instability theory discussed in MP21 in order to provide context for the discussion to follow that begins in Section 3.

The theory of MP21 considers the evolution of the stratified turbulence that develops in a background state in which the stratifications of temperature and salinity lie in the diffusive-convection regime. In this circumstance it is assumed that the average effect of micro-scale stratified turbulence on the larger scale background can be adequately captured by the effective turbulent diapycnal diffusivities for temperature K_Θ and salinity K_S. It is then further assumed that both K_Θ and K_S are only dependent upon the buoyancy Reynolds number Re_b of the system so that the governing mean field equations for the 1D averaged temperature profile $\Theta(z,t)$ and salinity profile $S(z,t)$ have the forms:

$$\begin{aligned} \frac{\partial \Theta}{\partial t} &= -\frac{\partial}{\partial z} F_\Theta = \frac{\partial}{\partial z}(K_\Theta(Re_b)\frac{\partial \Theta}{\partial z}) \\ \frac{\partial S}{\partial t} &= -\frac{\partial}{\partial z} F_S = \frac{\partial}{\partial z}(K_S(Re_b)\frac{\partial S}{\partial z}) \end{aligned} \tag{1}$$

In the above equations, Θ and S are defined in density units so that the equation of state can be written as: $\rho = \rho_0 + S - \Theta$.

It is furthermore assumed that the system is initially characterized by uniform gradients $\overline{\Theta}(z, t = 0) = -\Theta_{z0} z$ and $\overline{S}(z, t = 0) = -S_{z0} z$ so that the initial state which determines a background density ratio $R_\rho = S_{z0}/\Theta_{z0}$. $\Theta(z)$ and $S(z)$ at later times can then be decomposed into a combination of background fields $\overline{\Theta} = -\Theta_{z0} z$, $\overline{S} = -S_{z0} z$ and weak perturbations Θ', S', as:

$$\begin{aligned} \Theta(z) = &\quad \overline{\Theta}(z) + \Theta'(z) \\ S(z) = &\quad \overline{S}(z) + S'(z) \end{aligned} \tag{2}$$

These perturbations $\Theta'(z)$ and $S'(z)$ will then leads to a variation of Re_b by the amount

$$Re_b' = \frac{\partial Re_b}{\partial \rho_z} \frac{\partial \rho'}{\partial z} = \frac{\rho_0}{\nu g} \frac{\epsilon_0}{(\frac{\partial \overline{\rho}}{\partial z})^2} \frac{\partial \rho'}{\partial z} = -\overline{Re_b} \frac{\frac{\partial S'}{\partial z} - \frac{\partial \Theta'}{\partial z}}{\frac{\partial \overline{\rho}}{\partial z}} \tag{3}$$

which feeds back on the time-evolution of $\Theta(z)$ and $S(z)$ through the governing equations (1). Positive feedback for certain modes will lead to the general instability of the system. By expanding the perturbations in normal modes $(\Theta', S') = (\hat{\Theta}, \hat{S}) \exp(\lambda t) \exp(ikz)$ in (1) the original equation set (1) will be transformed to an eigenvalue problem with the growth-rate λ as the eigenvalue of the resulting 2 by 2 matrix. The value of λ is then determined by solving the quadratic equation resulting in:

$$\begin{aligned} &\lambda^2 + k^2 (K_\theta + K_s + \frac{\partial K_s}{\partial Re_b} Re_b \frac{R_\rho}{R_\rho - 1} - \frac{\partial K_\theta}{\partial Re_b} Re_b \frac{1}{R_\rho - 1}) \lambda \\ &+ k^4 (K_\theta K_s + \frac{\partial K_\theta}{\partial Re_b} K_s Re_b \frac{1}{R_\rho - 1} - \frac{\partial K_s}{\partial Re_b} K_\theta Re_b \frac{R_\rho}{R_\rho - 1}) = 0 \end{aligned} \tag{4}$$

A positive value of λ, which represents instability of the system, will be obtained if and only if the following criterion is satisfied:

$$K_\theta K_s + \frac{\partial K_\theta}{\partial Re_b} K_s Re_b \frac{1}{R_\rho - 1} - \frac{\partial K_s}{\partial Re_b} K_\theta Re_b \frac{R_\rho}{R_\rho - 1} < 0 \tag{5}$$

if we assume that K_S and K_θ have a local power law dependence on Re_b as $K_S \sim Re_b^{\beta_s}$ and $K_\Theta \sim Re_b^{\beta_\theta}$, the above criterion will be simplified to:

$$\beta_s - 1 > \frac{\beta_\theta - 1}{R_\rho} \tag{6}$$

Therefore the precise criterion for the instability depends on the details of the parametrization scheme that is employed to describe the dependence of the turbulent diffusivities upon the buoyancy Reynolds number in the stratified turbulent flow. In MP21 we employed the

empirically calibrated parametrization scheme for single-component fluids of [28] as the candidate parametrization based on the somewhat bold assumption that the temperature and salinity field will be relatively independent in the state and therefore this pair of single-component parametrizations should provide an accurate description of the doubly diffusive turbulent system. The effectiveness of this description will be tested in section 4.2 of the current paper below and a more general calibration of the parametrization for the diffusive-convection system will be performed and compared with the current assumption in the work that will be discussed in detail elsewhere. The specific functional form of [28]s parametrization scheme is as follows:

$$\begin{aligned}
K_\rho^{BB}(Re_b, Pr) = &\quad \kappa, &&\text{for } Re_b < 10^{\frac{2}{3}} Pr^{-\frac{1}{2}} \\
K_\rho^{BB}(Re_b, Pr) = &\quad \frac{0.1}{Pr^{\frac{1}{4}}} \nu Re_b^{\frac{3}{2}}, &&\text{for } 10^{\frac{2}{3}} Pr^{-\frac{1}{2}} < Re_b < (3ln\sqrt{Pr})^2 \\
K_\rho^{BB}(Re_b, Pr) = &\quad 0.2\nu Re_b, &&\text{for } (3ln\sqrt{Pr})^2 < Re_b < 100 \\
K_\rho^{BB}(Re_b, Pr) = &\quad 2\nu Re_b^{\frac{1}{2}}, &&\text{for } Re_b > 100
\end{aligned} \tag{7}$$

If we substitute $Pr = 700$ and $Pr = 7$ into the above equations to obtain the forms of $K_S(Re_b)$ and $K_\Theta(Re_b)$ separately, the criterion described in (6) can be evaluated to obtain the following condition:

$$0.17 < Re_b < 97 \tag{8}$$

Once this criterion is satisfied, the layering mode of instability will continually grow until a diffusive-convection staircases is fully formed, as has demonstrated by the no linear mean-field model simulation in MP21. However, as will be discussed in detail in what follows, we will employ a more moderate value of Prandtl number $Pr = 70$ (or Schmitt number $Sc = 70$) for salinity in the DNSs to be discussed herein due to the constraints on computational resources. In this circumstance, parametrization of [28] gives a different formula for the salinity diffusivities which will lead to a revised Re_b criterion of:

$$0.55 < Re_b < 41 \tag{9}$$

While (8) is still the criterion that should be applied into the real oceanographic environment, the effectiveness of the theory needs to be tested based in our DNS is criterion (9), under the choice of parameters in the current model. The goal of the analyses we will proceed to

describe is to demonstrate that the theory for staircase formation that we have demonstrated to explain the appearance of such structures in a mean field theory is verified in fully three-dimensional turbulent flow.

DIRECT NUMERICAL SIMULATIONS

In this section we discuss the design of DNS analyses to be employed to study the development of the layering structures that form from the Re_b instability. In what follows, we will firstly discuss the governing equations and critical physical quantities in section 3.1. Then, in Section 3.2 we will discuss the detailed numerical settings of our DNS analyses.

Governing equations and physical quantities

In order to develop a state of homogeneous stratified turbulence in the diffusive-convection regime consider the temperature $\Theta(x,y,z,t)$ and salinity $S(x,y,z,t)$ fields to be determined by a background temperature and salinity characterized by negative vertical gradients Θ_{z0} and S_{z0} and perturbation fields $\Theta^{pt}(x,y,z,t)$ and $S^{pt}(x,y,z,t)$, namely:

$$\begin{aligned} \Theta(x,y,z,t) &= \Theta_{z0} z + \Theta^{pt}(x,y,z,t) \\ S(x,y,z,t) &= S_{z0} z + S^{pt}(x,y,z,t) \end{aligned} \tag{10}$$

Subject to the Boussinesq approximation, the scalar fields $\Theta^{pt}(x,y,z,t)$, $S^{pt}(x,y,z,t)$ and the velocity field $\boldsymbol{u}(x,y,z,t) = (u(x,y,z,t), v(x,y,z,t), w(x,y,z,t))$ will be governed by the Navier-Stokes equation as in:

$$\begin{aligned} \frac{\partial \boldsymbol{u}}{\partial t} + \boldsymbol{u}\cdot\nabla\boldsymbol{u} &= -\boldsymbol{\nabla} p - J\left(\frac{R_\rho}{R_\rho - 1} S^{pt} - \frac{1}{R_\rho - 1}\Theta^{pt}\right)\boldsymbol{e_z} + \frac{1}{Re}\nabla^2\boldsymbol{u} + \mathbf{F} \\ \boldsymbol{\nabla}\cdot\boldsymbol{u} &= 0 \\ \frac{\partial \Theta^{pt}}{\partial t} + \boldsymbol{u}\cdot\nabla\Theta^{pt} &= \frac{1}{RePr}\nabla^2\Theta^{pt} + w \\ \frac{\partial S^{pt}}{\partial t} + \boldsymbol{u}\cdot\nabla S^{pt} &= \frac{1}{ReSc}\nabla^2 S^{pt} + w \end{aligned} \tag{11}$$

where $\boldsymbol{e_z}$ is the unit vector in the positive vertical direction. We have non-dimensionalized above equations using the length scale L_0, velocity scale U_0, temperature scale $\Delta\Theta = |\Theta_{z0} L_0|$, salinity scale $\Delta S = |S_{z0} L_0|$ and density scale $\Delta\rho = \Delta S - \Delta\Theta$.

The critical non-dimensional parameters are the Reynolds number Re, bulk Richardson number J, inverse density ratio R_ρ, Prandtl number Pr and Schmitt number Sc, which can then be defined explicitly as:

$$\begin{aligned} Re &= \frac{U_0 L_0}{\nu} \\ J &= \frac{g\Delta\rho L_0}{\rho_0 U_0^2} = \frac{g(\Delta S - \Delta\Theta)L_0}{\rho_0 U_0^2} \\ R_\rho &= \frac{\Delta S}{\Delta\Theta} \\ Pr &= \frac{\nu}{\kappa_\theta} \\ Sc &= \frac{\nu}{\kappa_s} \end{aligned} \tag{12}$$

where ν is the kinematic viscosity, κ_θ and κ_s are molecular diffusivities for heat and salt and ρ_0 is the reference density. We also assume that the system is subject to an external body forcing $\mathbf{F}$ whose specific form will be discussed in detail in the next subsection.

Based on (11), we can straightforwardly derive the time-derivative of the volume-averaged kinetic energy of the system $KE \equiv 1/2\langle|\mathbf{u}|^2\rangle$ as (here $\langle\cdot\rangle$ represents the volume averages):

$$\frac{dKE}{dt} = P - (F_{b\theta} + F_{bs}) - \epsilon \tag{13}$$

where

$$\begin{aligned} P &= \langle \mathbf{u}\cdot\mathbf{F}\rangle \\ \epsilon &= \frac{1}{Re}\langle \frac{\partial u_i}{\partial x_i}\frac{\partial u_i}{\partial x_i}\rangle \\ F_{b\theta} &= -\frac{J}{R_\rho - 1}\langle w'\Theta'\rangle \\ F_{bs} &= \frac{JR_\rho}{R_\rho - 1}\langle w'S'\rangle \end{aligned} \tag{14}$$

are defined to be the energy input from external forcing, viscous dissipation ratio, buoyancy flux associated with temperature and salinity separately. In above equations, we decomposed any given field $f(x, y, z, t)$ into $f = \overline{f} + f'$, where the $\overline{f}$ represents the horizontal average of that field and f' represents perturbation to it. It should be noticed that the unstably stratified background temperature field continues to release energy to the system through the heat flux and $F_{b\theta} < 0$, meanwhile the energy of the system continues to be invested in mixing the stably stratified salinity gradient through the salt flux and $F_{bs} > 0$.

When the system remains in a quasi-steady state, the right-hand side of (13) should be approximately 0. Considering that the absolute value of buoyancy fluxes $F_{b\theta}$ and F_{bs} are

usually much smaller than the viscous dissipation ϵ in our system (as will be demonstrated below), the balance of the KE budget is mainly kept by the first and last term of the right hand side of (13), namely:

$$P \sim \epsilon \tag{15}$$

Because the value of ϵ directly controls the value of the Re_b of the system, the Re_b can be estimated through:

$$Re_b = \frac{Re}{J}\epsilon \sim \frac{Re}{J}P \tag{16}$$

By controlling the energy input rate P we can essentially control the buoyancy Reynolds number of the system, which allows us to test our criterion for staircase formation in Re_b instability theory which is based solely on Re_b.

Numerical Methods

Governing equations (11) are integrated in a triply-periodic cubic domain of length 2π using the open-source computational fluid dynamics software Nek5000 ([39]). Nek5000 was developed at Argonne National Laboratory based on the spectral element method (e.g. [40], [41]) which is especially suited to simulations of transitional and turbulent flow.

In order for the system to achieve a quasi-steady state, we choose to apply very similar initial fields and forcing with the settings in the recent body-forced simulations of [38]. Specifically the initial fields are defined as a superposition of randomly phased horizontal shear modes $\mathbf{u}_{shear}$ and randomly phased three-dimensional internal wave modes $(\mathbf{u}_{internal}, \Theta_{internal}, S_{internal})$. The shear modes are confined to large scale modes $m \leq m_c = 7$ only and amplitude for modes with vertical wavenumber m is allocated to be proportional $1/m$ in order to follows initial energy spectrum of m^{-2}. The detailed functional form of $\mathbf{u}_{shear}$ is as follows:

$$(u_{shear}, v_{shear}, 0) = \frac{1}{\sqrt{m_c}} \sum_{m=1}^{m_c} \frac{1}{m}(cos(\phi_m + mz), sin(\phi_m + mz), 0) \tag{17}$$

where ϕ_m is the phase chosen randomly for each vertical mode.

The form of these internal wave modes is initialized based upon the algorithm as discussed in Appendix b of [42] to satisfy the three-dimensional Garrett-Munk Spectrum. These internal wave modes only contribute 10% of the initial energy and they are only non-zero for

modes with $|\mathbf{k}| \leq 7$. For recent discussions of the Garrett-Munk spectrum of internal waves in the oceans and the ability of high-resolution ocean models forced by both the atmosphere and the astronomical tidal potential to replicate this spectrum see [43] and [44].

We first integrate the system without body-forcing to 20-time units in order for the energy contained in the initial larger scale modes to cascade to the small scales, a strategy previously employed in [38]. Then we begin to introduce body-forcing that has an appropriate form to represent the stochastic forcing of the large-scale modes. As employed in previous direct numerical simulations (e.g. [36], [37], [38]), these vortical modes of forcing only act on the horizontal component of the velocity and can be written in the following form:

$$(F_x, F_y) = A \sum_{(k,l)} A_{k,l}(l, -k) e^{i(kx+ly)} \tag{18}$$

where k and l are the wave numbers in the x and y directions respectively. The forcing is only non-zeros for modes whose horizontal wavenumber $k_h = \sqrt{k^2 + l^2}$ lies in the small parameter window of $2.5 \leq k_h \leq 3.5$, as optimized in [38]. The complex action for each mode $A_{k,l}$ is chosen randomly at each time step, after which a normalization constant A is determined such as to control the energy input rate P at each time step to be a constant (we used the method proposed by [37] to avoid accidental energy inputs due to the finite time step).

We have performed 6 different simulations that will be discussed in this paper, whose governing parameters are summarized in Table 1. While fixed values of $Re = 1000$, $J = 1$, $Pr = 7$ and $Sc = 70$ were employed for all these simulations, we vary the density ratio R_ρ for simulations 1-4 to investigate how R_ρ will influence the dynamics or the equilibrium state of the system. It will be important to note that $R_\rho \to \infty$ for simulation 4 is achieved by integrating the system in the single-component stratification case with $Sc = 70$. For the control simulation number 5, we switched the power P to the value 0.1 which leads to a larger value of $Re_b \sim 100$ that is well beyond the upper limit of the instability criterion. For the control experiment number 6, we double the vertical extent of the domain with $R_\rho = 5$ to investigate how the layer formation process is dependent upon this characteristic of the model.

For simulations other than simulation number 6 in the current paper, we first apply an intermediate resolution of $350 \times 350 \times 350$ grid points (for simulation number 6 in which

Numbering	L_z	P	R_ρ	Pr	Sc	Re	J
1	2π	0.01	2	7	70	1000	1
2	2π	0.01	5	7	70	1000	1
3	2π	0.01	8	7	70	1000	1
4	2π	0.01	∞	N.A.	70	1000	1
5	2π	0.1	2	7	70	1000	1
6	4π	0.01	5	7	70	1000	1

TABLE I. Governing parameters for the direct numerical simulations performed in this paper.

the vertical domain is doubled, the vertical resolution is also doubled to $350 \times 350 \times 700$ grid points) in the simulation domain. From a theoretical perspective this resolution that cannot reach the requirement of DNS as the mesh could not reach the Batchelors scale for the slower diffusing salinity. However, in order to represent the layer formation process both the large domain size and the long integration time is necessary for our simulations, which restricts the resolution that can be applied. In Appendix A, we compared simulations with different resolutions to show that the layer formation that we report in this paper is resolution independent. Once the steady layered structure forms in the numerical simulations (the corresponding time is marked as $t = t_1$), we then double the resolution in each direction (which gives $700 \times 700 \times 700$ grid points for simulations other than number 6) in the domain, which allows us to better resolve the structure of the staircase state that forms. This system is then integrated for a short time until the system stabilizes again at $t = t_2$. In what follows, we will first analyze the layer formation process that is characterized by the long integration of intermediate resolution in section 4, then we will analyze the staircase states in detail by focusing on the subsequent high-resolution evolution to be discussed in section 5.

SPONTANEOUS FORMATION OF THERMOHALINE STAIRCASES IN THE DIRECT NUMERICAL SIMULATIONS

In this section, we will focus on discussing the process of spontaneous formation of layered structures in our system. In section 4.1 we will first describe the evolution of the system in

each different simulations to illustrate whether layers will form from the system and how the layer formation processes depend on different values of Re_b and R_ρ. Then in section 4.2 we will provide a detailed comparison between the layer formation process in the simulations with the linear growth-rate derived from section 2. By doing this we will be able to evaluate whether the Re_b instability theory is indeed dominating the non-linear evolution process of direct numerical simulations. It will be important to recognize that the discussion in this section is confined to the layer-formation phase of the evolution that is characterized by time $t \leq t_1$.

Thermohaline layering state in the direct numerical simulations

In our simulations, well-defined layered structures form spontaneously in all simulations except for simulation number 5 in which a stronger forcing is applied. As an example, the layer formation process for simulation number 1 is illustrated in Figure 1, in which we show the state of the temperature and salinity fields in pseudo-color plots (a-f) and the horizontally averaged vertical profiles (g-i). At $t = 100$, the constant energy input from the vortical mode forcing keeps the system in a homogeneously stratified turbulent state in which the temperature and salinity fields remain in the linear-gradient configuration. After a long integration time, the first sign of the formation of the vertical structure occurs at approximately $t_i = 1000$ (t_i represents the time that the initial layering structure forms). As shown in Figure 1 (b,e,h), the system develops into a four-step staircase state at this time of the evolution. These four-step staircases then gradually merge together to form a well-defined two-step layered state at approximately t_m=2100 (t_m represents the time that the layers merge into higher steps in our system), which is then retained in the system until the end of the simulation at $t_1 = 3098$. The layered state at $t = t_1$ is illustrated in Figure 1 (c,f,i). By comparing Figure 1(h) and Figure 1(i), we can notice that the merged two-layer state has much sharper interfaces and more homogenized mixed layers compared with the four-step staircase. In what follows, we will use the phrase staggered layered state to describe the layered state that are not very well shaped as in Figure 1(h).

These different phases of evolution of the layer formation process can also be viewed in the time variation of $F_{b\theta}$ and F_{bs} depicted in Figure 2. In this Figure, three different phases, namely the initial staircase formation stage, layer merging stage and equilibrium stage are

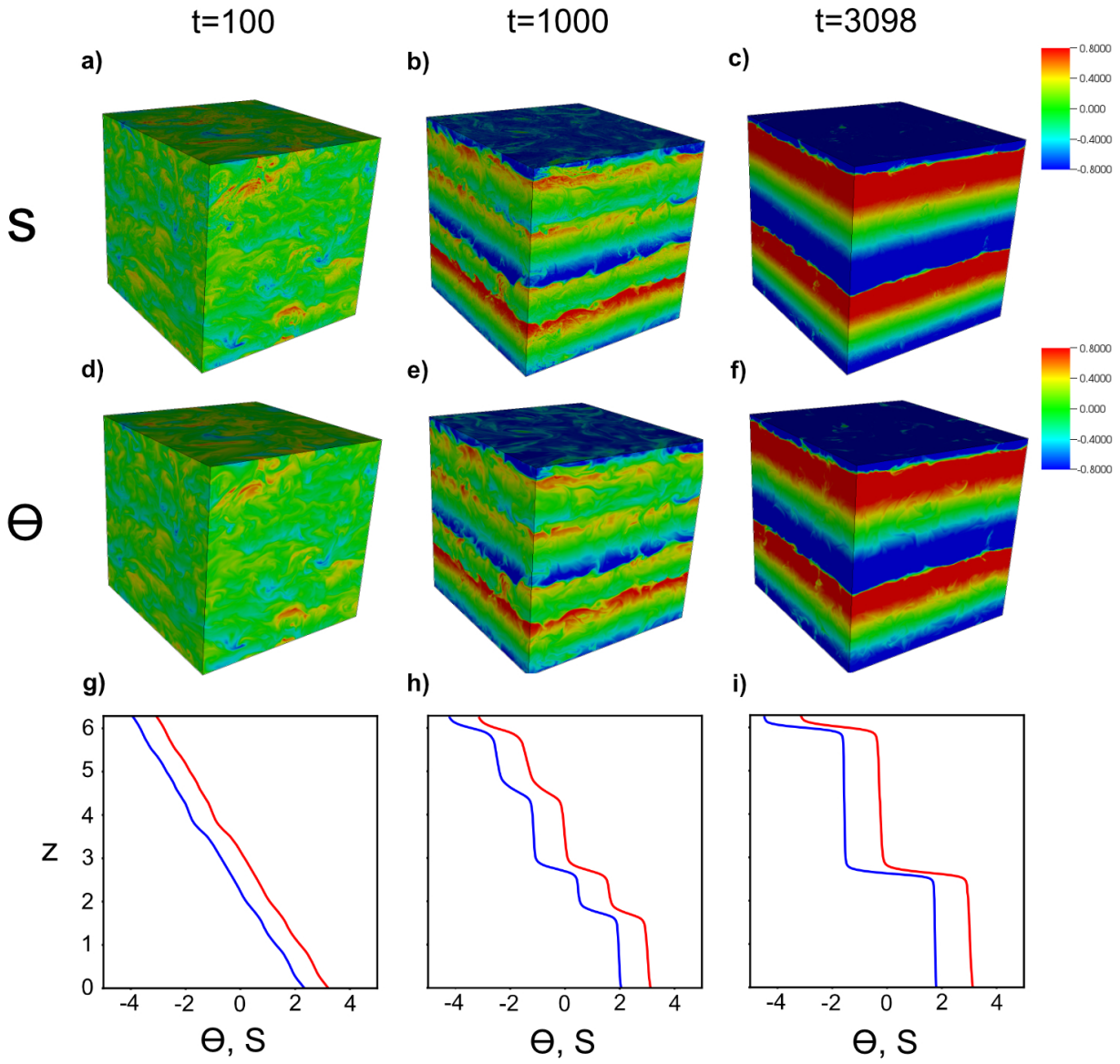

FIG. 1. In Figures (a-f) we show the pseudo-color plots of the salinity field $S^{pt}(x, y, z, t)$ (a-c) and the temperature field $\Theta^{pt}(x, y, z, t)$ (d-f) at three different time slices $t = 100$, $t = t_i = 1000$, $t = t_i = 3098$ for simulation number 1. In Figures (g-i) we plot the horizontally averaged profiles of salinity $\overline{S}(z)$ (blue) and temperature $\overline{\Theta}(z)$ (red) as a function of depth for the same time slices.

separated by three characteristic time (t_i, t_m, t_1) which are denoted using the vertical lines. Generally speaking, both $|F_{b\theta}|$ and $|F_{bs}|$ experience a continuous increase during the layer formation stage and layer merging stage and become stabilized in the final equilibrium stage of evolution. This trend of increasing $|F_{b\theta}|$, $|F_{bs}|$ as layers form and merge is consistent

with previous numerical simulations of thermohaline staircases of the salt-fingering system ([13]) and the low-Pr diffusive-convection system ([45]). Meanwhile, the net buoyancy flux $F_b = |F_{bs}| - |F_{b\theta}|$ keeps decreasing in the layer formation stage and layer merging stage, so that F_b changes from positive values to negative values in the entire evolution process. As we will show in the next subsection, this increase of energy flow to the kinetic energy reservoir will lead to an increase of viscous dissipation in the system.

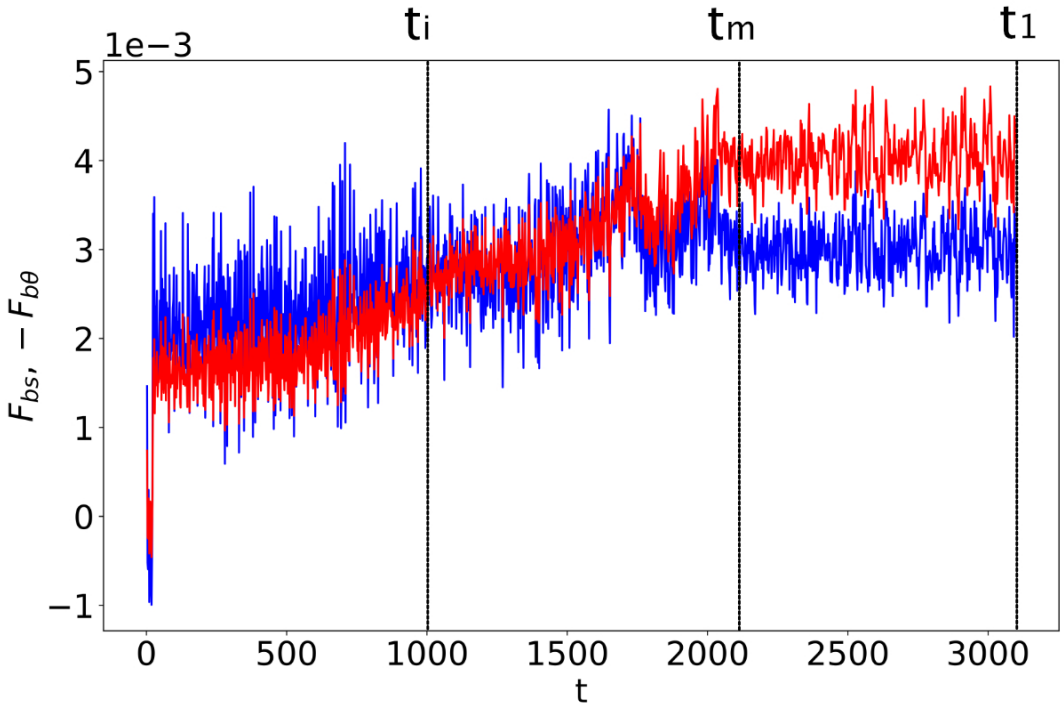

FIG. 2. Evolution of the temperature induced buoyancy flux $F_{b\theta}$ (red) and salinity induced buoyancy flux F_{bs} (blue) in the evolution of simulation number 1. Temperature induced buoyancy flux is plot with the absolute (negative) value for comparison. The three characteristic times t_i, t_m and t_1 represent the time that the first layered structure forms, the time that well-defined layers form and the end of the intermediate resolution simulation respectively (their definitions are discussed in details in the text).

The above-described evolution process generally applies also for simulations number 2-4 (which corresponds to $R_\rho = 5$, $R_\rho = 8$ and $R_\rho = \infty$ separately). In these simulations, however, the firstly formed staggered layered state has two steps, which then merge into the single-step layered state so that the mixed layers that forms occupies almost the entire

domain. Such evolution can be seen the pseudo-color plot for the salinity field $S^{pt}(x, y, z, t)$ for simulation number 2 (as an example) at the initially formed staggered layered stage ($t = t_i = 1500$) and merged layered stage ($t = t_m = 5000$) in Figure 3 (a,b). In order to test whether the layer formation process in the simulations is dependent upon the height of the domain, we compare the staircase state formed in simulation number 2 (this will be referred to as "normal box") with that in simulation number 6 that has twice the vertical domain height (this will be referred to as "tall box") while all other conditions remain the same. In the tall box simulation shown in Figure 3(c,d), the staircases formed are somewhat unevenly distributed with step-sizes varying at different vertical levels. There are 5 steps formed at time $t = 1500$ which later merged into 3 steps at $t = 5000$. This makes the averaged step-sizes slightly lower but comparable with that of the normal box simulation at both these time-slices. Furthermore, the turbulence characteristics also appear similar for the normal box domain and the tall box domain as can be seen in Figure 3. Therefore we conclude that the time-scale and the length-scale of the staircase formation are not sensitive to the vertical domain height we have chosen. For this reason we will only discuss the $R_\rho = 5$ simulated in the normal box to be consistent with other simulations in what follows. It is worth mentioning here that although the 3-step configuration shown in Figure 3(d) is stable within our integration time of 6500 time units, we dont rule out the possibility that these staircases will eventually merge if this simulation is integrated much longer.

The important quantities for the layer formation and layer merging process are summarized in dimensional units in Table II. The unit transformation is made by relating the controlled non-dimensional viscous dissipation rate with the typical value of viscous dissipation $\epsilon = 5 \times 10^{-9} W/kg$ (see [29] for example) in the Canada Basin. Using the typical value of molecular viscosity of $\nu = 1.8 \times 10^{-6} m^2/s$ in the Arctic Ocean, we calculate the characteristic length-scale for simulation numbers 1-4 to be approximately $L_0 = 0.33m$ and a time scale $L_0/U_0 = 60s$. After transforming the characteristic times to physical units as shown in Table II, we can see that it takes a timescale of several days for the layered structure to develop and merge into an equilibrated staircase. The step-size L of these equilibrium staircase structures in our simulation has the physical length scale of approximately 1m. This is consistent with the measurements of the staircases in the Arctic Ocean, whose step-sizes typically range from 1m-5m (e.g. [19]). This also shows that the choice of our vertical domain height in the numerical simulations is capable of capturing the real

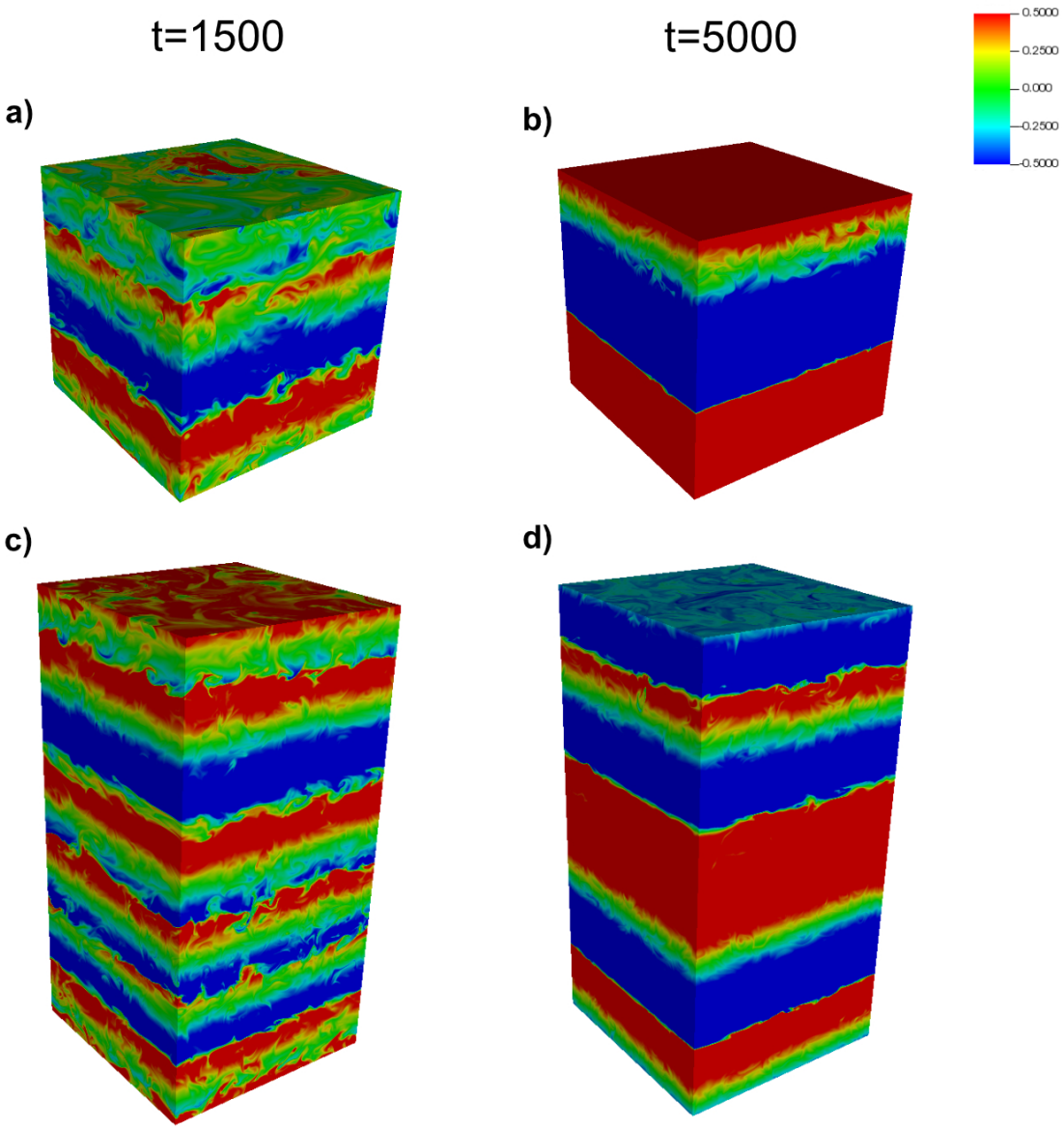

FIG. 3. Pseudo-color plots of the salinity field $S^{pt}(x, y, z, t)$ for simulation with $R_\rho = 5$ at time slices $t = t_i = 1500$ (a,c) and $t = t_m = 5000$ (b,d). Figure (a,b) shows the normal box simulation for simulation number 2 and Figure (c,d) shows the tall box simulation for simulation number 6.

staircases formed in the Arctic Ocean. The interfacial thicknesses $h_{I\theta}$ and h_{Is} formed in our simulations have been evaluated as the depth-range within which $|\Theta_z| > 1$ and $|S_z| > 1$ are satisfied separately. The interfacial thicknesses have the order of 0.1m, with the temperature interfaces generally thicker than the salinity interfaces due to the higher molecular

#	P	R_ρ	Re_b	Layering	Steps	t_i(day)	t_m(day)	t_1(day)	t_2(day)	$L(m)$	$h_{I\theta}(m)$	$h_{Is}(m)$
1	0.01	2	9.5	Yes	4→2	0.7	1.5	2.15	2.23	0.6	0.07	0.05
2	0.01	5	8.8	Yes	2→1	0.9	3.6	5.05	5.12	1.3	0.11	0.08
3	0.01	8	8.8	Yes	2→1	0.8	3.1	3.16	3.20	1.3	0.12	0.09
4	0.01	∞	8.7	Yes	2→1	1.4	6.6	6.94	6.99	0.6.	N.A.	0.10
5	0.1	2	83.0	No	N.A	N.A	N.A	1.81	N.A	N.A.	N.A.	N.A.

TABLE II. Basic simulation results summarized for the five simulations performed. In this table, layering with "yes" or "no" indicates whether layered structure observed to form in the system. t_i, t_m represents the time that the initially (staggered) layered state form and the well-merged layered state is observed in the simulation respectively. L is the step-size in the finally merged layering state, $h_{I\theta}$ and h_{Is} are the interfacial thicknesses of the temperature profile and salinity profile in the equilibrium layered state.

diffusivity at the interface. These values match well with the interfacial thickness measured in the Canada Basin by [46], who found that the temperature interfacial thicknesses are about 0.15m. These consistencies in physical scales of the staircase structures suggest that the layered structures formed in our numerical simulations not only provide guidance for theoretical studies of the layer formation mechanism, but they are also physically relevant for the actual staircases observed in the Arctic Ocean.

Comparison between the layer formation process in DNS analyses and theoretical predictions of MP21

While we have shown that the thermohaline staircase structures do form naturally in our numerical system, in this subsection we will provide the analyses required to answer the question as to whether these layered structures form because of the mechanism discussed in MP21. In this process we will provide three tests on the basis of which to compare our numerical simulations with the theoretical predictions of MP21 in what follows. Firstly we will investigate whether the stability criterion derived in MP21 is consistent with the layer formation process observed in our numerical simulations. Secondly we will analyze whether or not the key assumption of the [28] parametrization scheme that lies at the heart

of the theory proposed in MP21 is operating in the current numerical system. Third we will investigate whether the growth rate of the layering mode in our system is equal to the growth-rate predicted by the linear stability analysis. As we will demonstrate in what follows, the Re_b instability theory of MP21 provides rather good predictions for all these three aspects of the layer formation process.

We will start by evaluating the instability criterion of MP21. As we have reviewed in section 2, the Re_b instability theory predicts the layering instability of the system to occur only when the buoyancy Reynolds number satisfies the criterion $0.55 < Re_b < 41$ for $Pr = 7$ and $Sc = 70$. In order to evaluate whether the instability criterion is satisfied, we show the evolution of Re_b in the five different simulations we have performed in Figure 5. As expected, the buoyancy Reynolds number of the system self-adjusts to the level of approximately $ReP/J = 1000P$ (as discussed in (16)) soon after the introduction of the vortical forcing at $t = 20$. Therefore only the first four simulations (with $P = 0.01$) have an Re_b that satisfies the instability criterion which is consistent with our observations that the layered structure forms and only forms in these 4 simulations. Furthermore, it should be noticed that the level of Re_b is slightly higher for $R_\rho = 2$ than for the other simulations with $P = 0.01$. This is a consequence of the fact that negative buoyancy flux arises in this case which provides an additional net energy source to be dissipated only at $R_\rho = 2$ (as has been mentioned before in Figure 2). The value of Re_b for each simulation is averaged for time periods of $t = 50$ to $t = t_i$ (which roughly captures the stage of layer growth) to be shown in Table II.

Next we turn to evaluate the effectiveness of the [28]parametrization in the current numerical system. To do this we need to compute the diapycnal diffusivities K_θ and K_S at different vertical depth of our system and evaluate whether they are strongly correlated with the local buoyancy Reynolds number Re_b. To reduce the influence of advection that varies strongly with time, we perform time-averages over a 40 (nondimensional) time-unit interval to obtain the time-averaged vertical profiles on the basis of which to evaluate Re_b, K_Θ and K_S as follows:

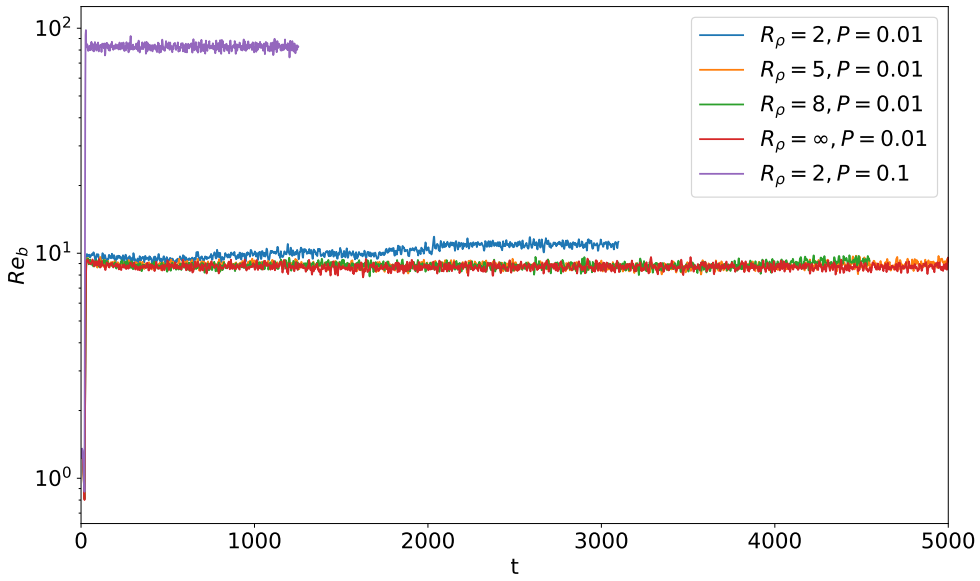

FIG. 4. Evolution of the volume averaged buoyancy Reynolds number in simulation number 1-5.

$$
\begin{aligned}
Re_b(z) &= \frac{Re\langle\epsilon(z)\rangle_t}{J} \\
F_\Theta(z) &= \langle\overline{w'\Theta'}(z)\rangle_t - \frac{1}{RePr}\frac{\partial\langle\overline{\Theta}(z)\rangle_t}{\partial z} \\
F_S(z) &= \langle\overline{w'S'}(z)\rangle_t - \frac{1}{ReSc}\frac{\partial\langle\overline{S}(z)\rangle_t}{\partial z} \\
K_\Theta(z) &= -\frac{F_\Theta(z)}{\frac{\partial\langle\overline{\Theta}(z)\rangle_t}{\partial z}} \\
K_S(z) &= -\frac{F_S(z)}{\frac{\partial\langle\overline{S}(z)\rangle_t}{\partial z}}
\end{aligned}
\tag{19}
$$

In the above equations, the overline represents the horizontal averages (this is different with background stratification defined in equation (10)) and $\langle\cdot\rangle_t$ represents the time averages over the chosen time-intervals. $F_\Theta(z)$ (or $F_S(z)$) are the total vertical heat (or salt) fluxes which include the contribution from both the convective fluxes and the diffusive fluxes.

In Figure 5, we showed the correlation between diapycnal diffusivities $K_\Theta(z)$, $K_S(z)$ and $Re_b(z)$ at $t = 0.5t_i$ for simulations 1-4 ($t = t_1$ for simulation number 5), namely at half the time needed for the first layering state to form in these simulations. These depth-dependent data are averaged in 50 small depth-intervals and plotted in the (Re_b, K) parameter space to be compared with the [28]'s parametrization evaluated from (7) in Figure 5. It can be

clearly seen in this figure that the distribution of Re_b at different depths spans approximately an order of magnitude due to the growth of perturbations in the system. In such a wide range of Re_b the diapycnal diffusivities $K_\Theta(z)$, and $K_S(z)$ follow very well the predictions of [28], except for slight deviations in the small Re_b regions for $K_\Theta(z)$. Most importantly the key element of the [28] parametrization needed to support the theory of MP21, namely the existence of the buoyancy-controlled regime for $K_S(z)$ that scales as $Re_b^{3/2}$ is well captured in the current system as shown in Figure 5(b). This fact shows that, in the process of the initial layering formation, the [28] does function in the way that we have described in the MP21 theory. This strongly implies that the theoretical derivations in MP21 are based on reasonable assumptions which are clearly confirmed in our current numerical system.

Finally, we will perform a detailed analysis of the vertical wavenumber spectrum for temperature/salinity for comparison with the theoretical predictions of MP21 for the growth rate of the layering mode of instability. Specifically, we perform the vertical Fourier transformation off the horizontally averaged salinity field (or temperature field) following:

$$\begin{aligned} S_m(t) &= \frac{1}{V}\int_V S(x,y,z,t)e^{imz}dV \\ \Theta_m(t) &= \frac{1}{V}\int_V \Theta(x,y,z,t)e^{imz}dV \end{aligned} \tag{20}$$

where m must take integer values as constrained by our triplet periodic domain with size 2π. In Figure 6(a-d) we show the evolution of the vertical wavenumber spectrum of salinity S_m (temperature spectrum is similar) for the four simulations in which staircases formed. The evolution of the spectrum confirms our observations described in the last subsection concerning the different stages of the evolution: for $R_\rho = 2$ shown in Figure 6(a). The system is first dominated by the $m = 4$ mode at $t = t_i$ when the system has a staggered layered structure (see Figure 1(h)). At $t = t_m$, the growth of the m=2 mode finally dominates the system and stays steady, which represents the formation of the stable two-layer staircase state. We can also see the formation of the two-layer state for $R_\rho = 5$, $R_\rho = 8$ and $R_\rho = \infty$ before the final formed single-layer staircase in Figure 6(b)(c)(d). For comparison simulation number 5, however, there is no sign of layer formation as can be seen in Figure 6(e).

The evolution of the vertical wavenumber spectrum can also be compared with the growth-rate predicted by the theory based on the Re_b and R_ρ for each simulation. These linear growth-rates are represented as the dashed lines in Figure 6 (a-d). It can be seen from

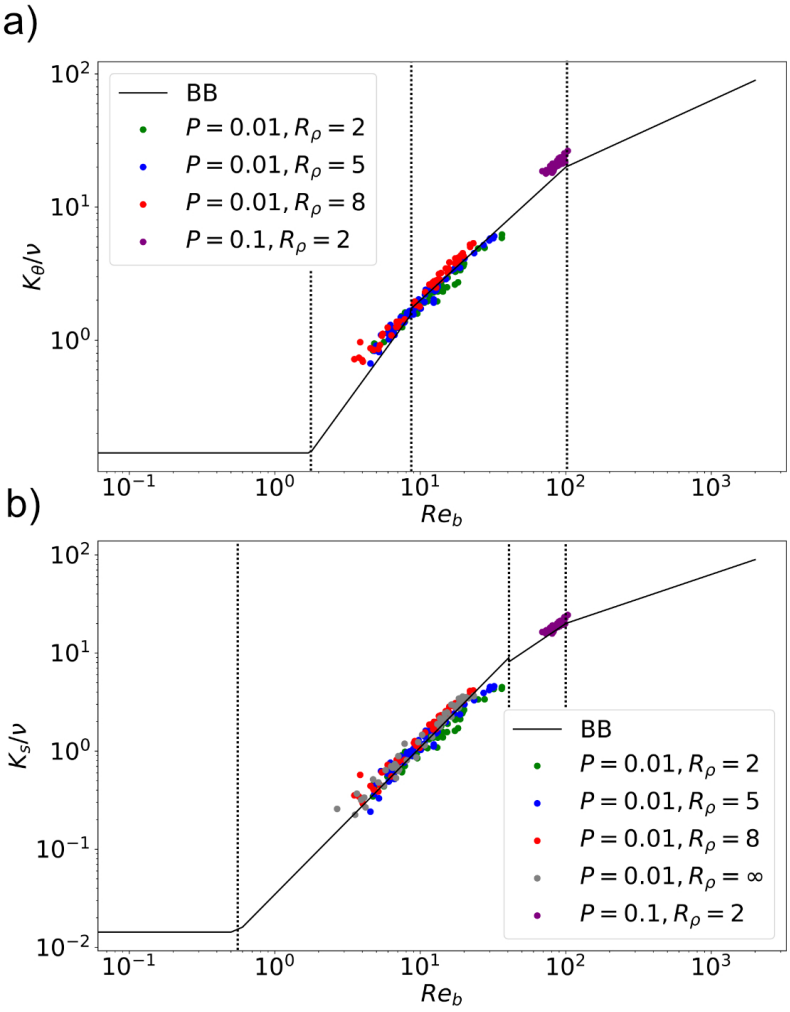

FIG. 5. Scatter plot of $(Re_b(z), K_\Theta(z))$ (a) and $(Re_b(z), K_S(z))$ at (Re_b, K) parameter space different vertical coordinates (b) evaluated for time-averaged at $t = 0.5t_i$ for simulation number 1-4 and at $t = t_1$ for simulation number 5. The black solid line shows the parametrization scheme of (7) for temperature Pr=7 (a) and salinity Sc=70 (b). The vertical dotted lines represent the critical Re_b values that separate different parametrization regions in (7).

the figure that the theory of MP21 offers a fairly good prediction for the growth of the first two vertical modes $m = 1$ and $m = 2$ before saturation. This fact provides further strong support for the effectiveness of the theory of MP21.

To summarize the results of this section, we have demonstrated the effectiveness of the Re_b instability theory from three perspectives. First we demonstrated that the instability

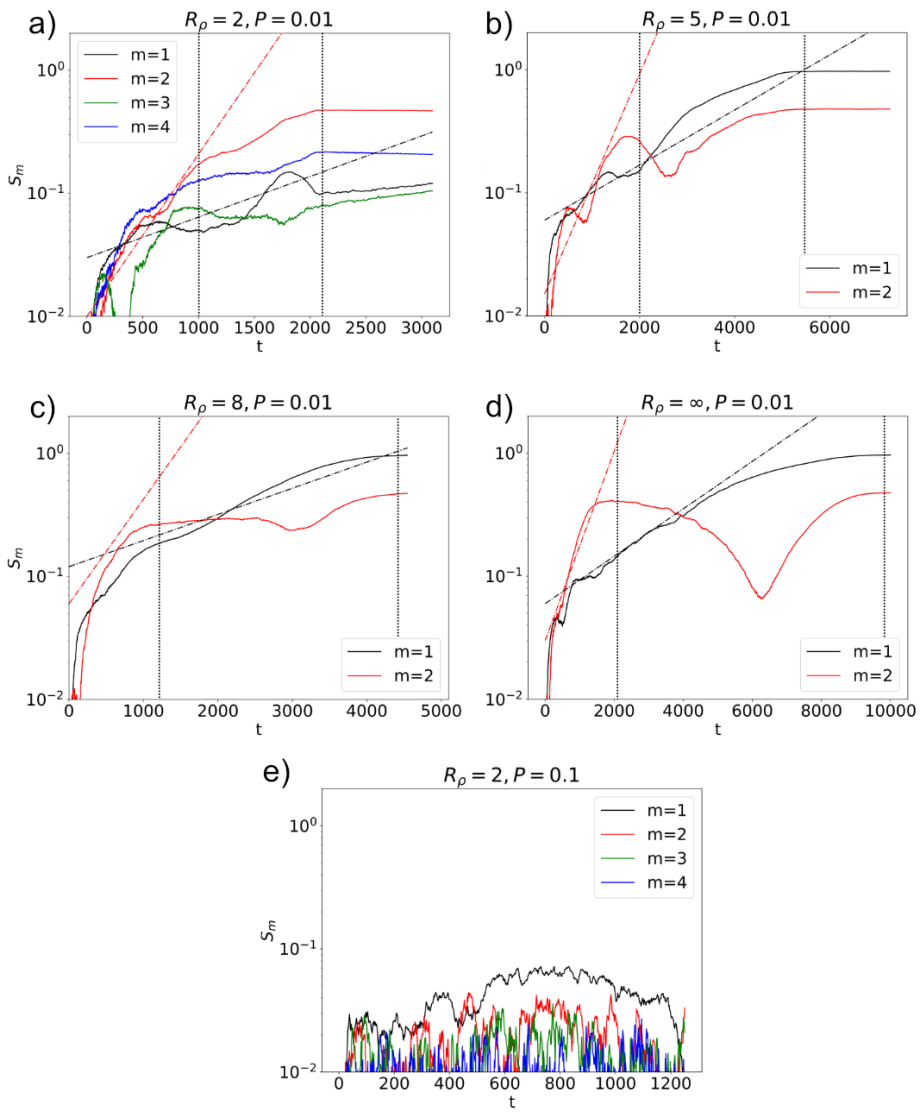

FIG. 6. Evolution of the vertical spectrum of salinity for various mode S_m as a function time in simulation number 1-5. The dot-dashed line (in (a)-(d)) represents the growth-rate λ for each mode predicted from the linear stability analysis calculated from formulae (4). The vertical dotted line (in (a)-(d)) marks the characteristic time t_i and t_m sequentially.

criterion provided correct predictions of whether the layers would form in the system. Secondly we showed that the key assumption of the parametrization scheme of [28] provides an accurate description of the vertical variations of the system. Finally we have demonstrated that the growth of the governing layering mode is consistent with the prediction of the linear stability analysis. Therefore, we conclude that the spontaneous formation of the layered structure in our system is indeed triggered by the Re_b instability theory described by MP21.

513 It should also be clear on the basis of the previous discussions that while Re_b solely
514 determines whether the layered structure will form in the DNS system, it seems that R_ρ
515 plays a role in determining the step-size of the initially formed layering mode, considering
516 that the number of layers formed in our simulations varies with R_ρ. The explanation of
517 the depth of the firstly formed layers in the system is not predictable on the basis of MP21
518 and goes beyond the scope of the current paper. In order to fully understand this problem,
519 we need a multi-scale model that captures the response of gradients at smaller scales, an
520 example of which is provided in the work of [16] that focused upon the salt-fingering regime
521 of doubly diffusive convection.

522 DIFFUSIVE CONVECTION STAIRCASE STRUCTURE IN THE DIRECT NU-
523 MERICAL SIMULATIONS

524 As we have demonstrated above, the thermohaline staircase structures form sponta-
525 neously in our continuously forced system. A natural and critical further objective of the
526 present work is to analyze the detailed steady structure of the diffusive convection staircases
527 that are formed. In order to achieve this, we have integrated the staircase state of the system
528 ($t = t_1$) with doubled resolution for an additional short period of time (summarized in Table
529 2) until the system reaches its steady state with the higher resolution, which is denoted as
530 time t_2. The better resolved domain allows us to look closely at the morphology and the
531 vertical transport, as will be discussed in section 5.1. In the following section 5.2, we will
532 compare our simulated interfaces with the existing theories of diffusive interfaces.

533 Staircase Structure

534 In Figure 7, we show the vertical cross-sections of the density field for simulations with
535 $R_\rho = 2, 5, 8$ separately. As discussed previously, while there forms the two-step layered state
536 with $R_\rho = 2$ at the end of our numerical simulation, simulations with $R_\rho = 5$ and $R_\rho = 8$
537 only has the single layer structure across the vertical domain. In all these simulations,
538 very sharp interface(s) and be clearly observed to separate well-mixed convective layers
539 below and above. Thin plumes can be observed in these fields to rise from the interfaces
540 to transport scalars into the mixed layers. These plumes have also been observed in the

previous numerical simulations of diffusive interfaces of [30], [47] and they have been argued as the crucial structure in transporting scalars from the interface into the mixed layers ([48]).

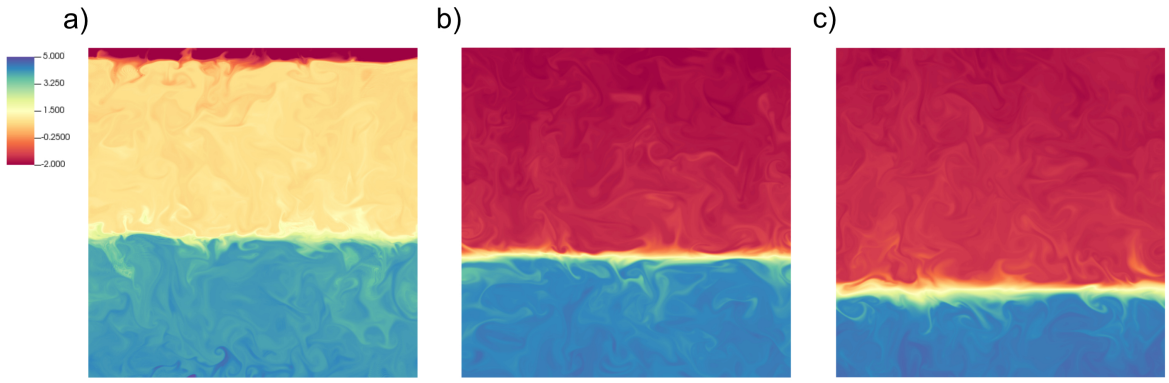

FIG. 7. Density fields for the equilibrium staircases at $t = t_2$ for simulation with $R_\rho = 2$ (a), $R_\rho = 5$ (b), $R_\rho = 8$ (c) separately. The pseudo-color plot is performed for the x-z plane at the y midpoint of the 3D domain.

In order to facilitate a further quantitive analysis of the layered structure, in Figure 8 we show the vertical distribution of heat/salt fluxes $(F_\Theta(z), F_S(z))$, vertical gradients of temperature/salinity $(\Theta_z(z), S_z(z))$ as well as the effective vertical diffusivities for temperature/salinity $(K_\Theta(z), K_S(z))$ (calculated as the ratio of the previous two sets of physical quantities) of the system, all evaluated based on averaged profiles in the steady state of the high-resolution run for our simulations with $R_\rho = 2, 5, 8$ separately. As shown in Figure 8 (c,f,i), the vertical diffusivities are significantly different in the mixed layers compared with the interface regions, suggesting entirely different dynamics in those vertical regions: in the mixed layers, mixing is driven by strong turbulent convection which leads to the same values of diffusivities for heat and salt. In the interface region(s), however, the turbulent diffusivities for heat and salt are of the same order as the molecular diffusivities for temperature and salinity, suggesting the absence of turbulent motions at the interface region. In fact, the turbulent diffusivities at the interfaces are much lower for $R_\rho = 5, 8$ compared with $R_\rho = 2$. This is possibly because the scalar variations across the interfaces are higher for $R_\rho = 5, 8$ compared with $R_\rho = 2$ (as shown in Figure 7), which makes it more difficult for the turbulent convection in the mixed layers to penetrate the interfaces.

Even though the vertical diffusivities in the mixed layer regions are 2-3 orders of magni-

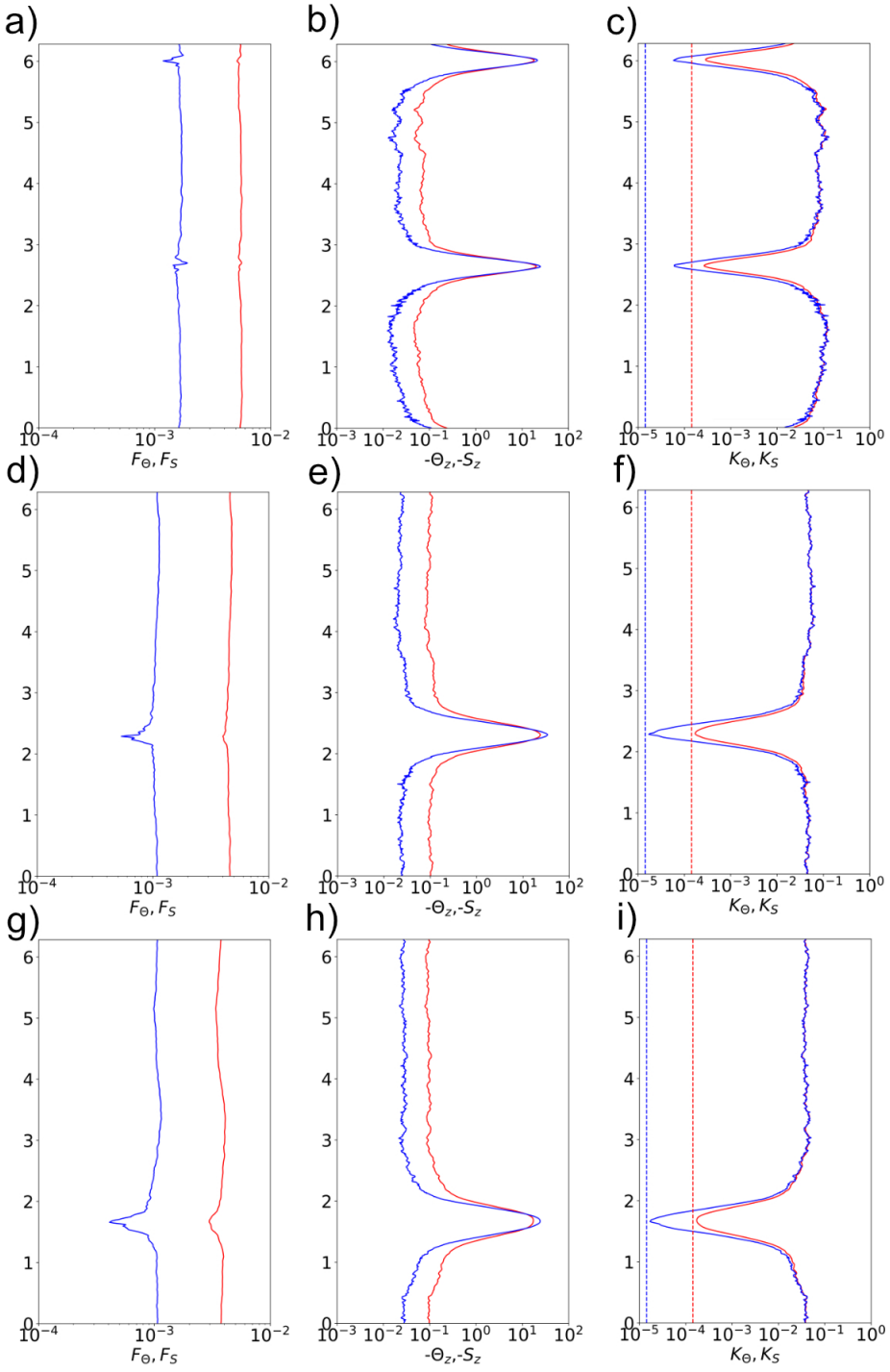

FIG. 8. Time averaged vertical fluxes for heat and salt $F_\Theta(z)$, $F_S(z)$, vertical gradients for temperature and salinity $\Theta_z(z)$, $S_z(z)$ and diapycnal diffusivities for heat and salt $K_\Theta(z)$, $K_S(z)$ as a function of depth for simulation with $R_\rho = 2$ (a,b,c), $R_\rho = 5$ (d,e,f), $R_\rho = 8$ (g,h,i) separately.

tude higher than in the interface regions, the vertical scalar gradients in the mixed layers are 2-3 orders of magnitude lower than in the interface regions (shown in Figure 8 (b,e,h)), which leads to the crude balance of vertical fluxes shown in Figure 8 (a,d,g). Specifically, while interface vertical fluxes are well balanced with mixed layer vertical fluxes with $R_\rho = 2$, the interface vertical fluxes are somewhat smaller than the mixed-layer vertical fluxes for $R_\rho = 5$ (Figure 8(d)) and $R_\rho = 8$ (Figure 8(g)), for both heat flux and salt flux. This mismatch suggests that the steady state for our simulations with $R_\rho = 5$ and $R_\rho = 8$ is in fact a quasi-equilibrium state and the system is still slowly evolving towards a true equilibrium state. Based on the equations of conservation of temperature/salinity:

$$\begin{aligned} \frac{\partial \overline{\Theta}(z)}{\partial t} &= -\frac{\partial F_\Theta(z)}{\partial z} \\ \frac{\partial \overline{S}(z)}{\partial t} &= -\frac{\partial F_S(z)}{\partial z} \end{aligned} \tag{21}$$

The relatively low fluxes at the interface will lead to the accumulation of scalars at the bottom of the interface and the depletion of scalars at the top of the interface. Therefore as time evolves this flux structure (smaller at the interface and higher in the mixed layer regions) will lead to a further enhancement of the scalar differences across the interface, which shows that the single layered structure for $R_\rho = 5$ and $R_\rho = 8$ are stable and the structure is becoming stabilized through time. In order to reach the full equilibrium state, another long period of simulation time is needed ($O(1000)$ time units) which is difficult to reach with our limited computational resources.

Comparison with the diffusive interface model of LS

While we have illustrated how the steady staircase structure is maintained by the balance of heat and salt flux between interface regions and mixed layers, we will compare these structures with the classical theoretical model of diffusive interfaces. LS presented a time-independent model of diffusive interfaces, which provides significant insights concerning the following theoretical and numerical simulations of diffusive interfaces studies (see review of [32], [45]). In this model, the interface consists of two boundary layers from which fluctuations arise on the outer edge of the interfaces and a diffusive core cross in which transport takes place only by molecular diffusion. This theoretical model describes a diffusive-interface structure that can only remain stable when the density ratio R_ρ is smaller than the critical

value of $R_\rho^{cr} = \tau^{-1/2}$. The LS model has later been extended by [49] and [50] to include the run-down evolution of the diffusive-interfaces in the $R_\rho > R_\rho^{cr}$ regime. As the diffusive interface structure is spontaneously formed and kept stable in our numerical simulations, the run-down model of [49] and [50] will be irrelevant to our current discussions. Therefore we will focus on comparing our interface structures only with the original time-independent model of LS.

To investigate whether the unstably stratified boundary layers are formed in our model as described in the LS theory, we plot in Figure 9 the horizontally averaged vertical density gradient, namely the buoyancy frequency, as follows,

$$N^2 = -\frac{1}{J}\frac{\partial\langle\overline{\rho}(z)\rangle_t}{\partial z} = -\frac{1}{J}\left(\frac{R_\rho}{R_\rho - 1}\frac{\partial\langle\overline{S}(z)\rangle_t}{\partial z} - \frac{1}{R_\rho - 1}\frac{\partial\langle\overline{\Theta}(z)\rangle_t}{\partial z}\right) \tag{22}$$

for $R_\rho = 2$, 5 and 8. In our system, $R_\rho^{cr} = \tau^{-1/2} = 3.16$ so that the small R_ρ simulation $R_\rho = 2$ satisfies the criterion while the large R_ρ simulations with $R_\rho = 5$ and 8 are outside the criterion. As shown in Figure 9(b,c), the unstably stratified boundary layers dont exist for the large R_ρ staircases (R_ρ=5 and R_ρ=8) considering that $N^2 > 0$ across the entire vertical domain. For $R_\rho = 2$, on the other hand, N^2 takes negative values in the mixed layer region. While this fact shows that the boundary layer structure is not that special in keeping the staircases stable in our model, it does not contradict the LS theory considering that the water columns do become unstably stratified below and above the interface core.

In order to further test whether the small R_ρ staircase that satisfies LSs criterion is consistent with their model, we need to evaluate the major predictions provided by this theory, in order for the interface structures to be stable. For this to be possible it is shown that density ratio at the interface R_ρ^I and the flux ratio at the interface γ^I are both required to be dependent solely on the molecular diffusivity ratio τ. Specifically their values have been predicted to be:

$$\begin{aligned} R_\rho^I &\equiv \frac{S_z}{\Theta_z} R_\rho|_{interface} = \frac{1}{\sqrt{\tau}} \\ \gamma^I &\equiv \frac{F_S}{F_\Theta} R_\rho|_{interface} = \sqrt{\tau} \end{aligned} \tag{23}$$

The above conclusions were derived in LS by making the assumption that the fluxes across the center of the interface are purely governed by molecular diffusion of heat and salt. As pointed out by [51] and developed in the recent work of [31], the molecular diffusivity in the LS theory should be replaced by the ratio of effective diffusivity across the interface

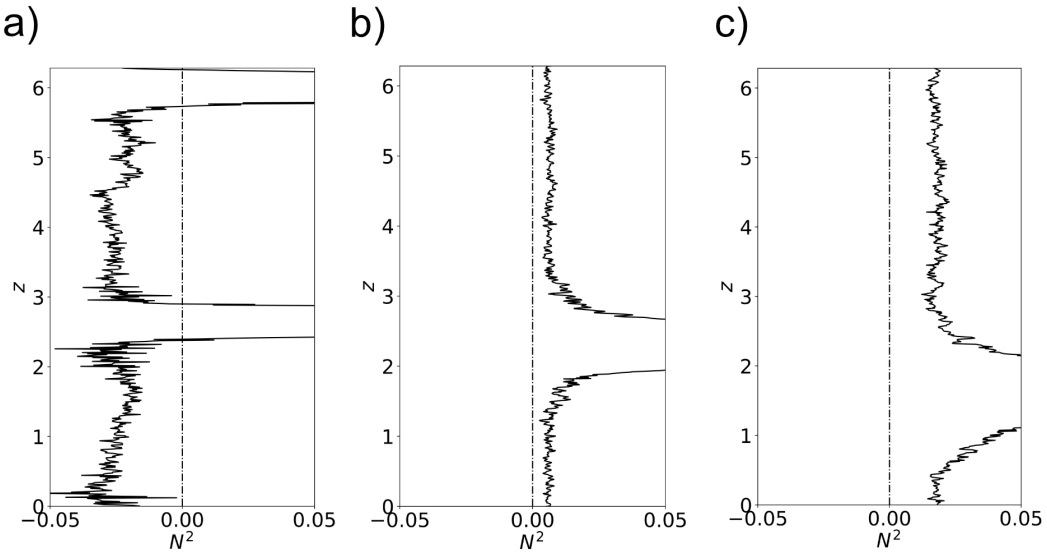

FIG. 9. Time averaged buoyancy frequency N^2 in the mixed layers as a function of depth for simulation with $R_\rho = 2$(a), $R_\rho = 5$ (b), $R_\rho = 8$(c) separately.

when the interface is influenced by turbulence. In our system, we have demonstrated that the effective diffusivities cross the center of the interface are close to but higher than the molecular values (see Figure 8 (c)). The ratio of the effective diffusivities $\tau^{eff} = K_S/K_\Theta$ at the interface are approximately 0.21 for both interfaces at $t = t_2$ for our simulation number 1, which is approximately twice the molecular value of 0.10. The predicted value for R_ρ^I and γ^I evaluated by substituting into τ^{eff} to (23) is $R_\rho^I = 2.2$ and $\gamma^I = 0.45$ separately. In Figure 10 we have plotted the (time-averaged) depth-dependent $R_\rho(z)$ and $\gamma(z)$ (solid lines) evaluated for our $R_\rho = 2$ simulation to be compared with the predicted value of R_ρ^I and γ^I at the interfaces (dashed lines). From this Figure it will be observed that the prediction of LS theory is lower for the estimate of interface R_ρ and higher for the estimate of interface γ, both with approximately 25% percent differences.

In order to understand why the LS model cannot provide an accurate description of our staircase simulations, two important distinctions between our numerical model and the original theoretical model of LS should be recognized: firstly, the theoretical model of LS assumed a perfectly homogenized mixed layers above and below the interfaces. As shown in our numerical model, however, a fully equilibrated staircase structure requires

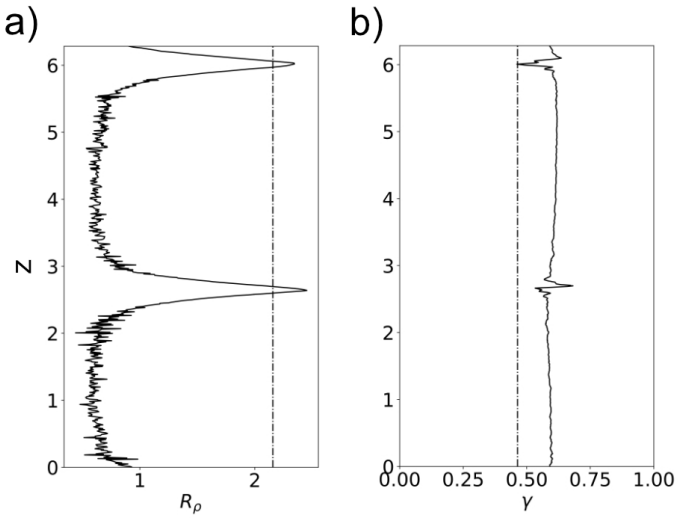

FIG. 10. Density ratio $R_\rho(z)$ (a) and flux ratio $\gamma(z)$ are plotted in the solid lines for simulation number 1 ($R_\rho = 2$), in comparison with the predicted value of R_ρ^I (a) and γ^I (b) from LSs theory in the vertical dashed lines.

finite values of vertical gradients (for both temperature and salinity) in the mixed layers. In this circumstance, as we have discussed above, the balance between vertical fluxes in the mixed layers and those in the interfaces are the key to maintain the staircase structure. This clearly goes beyond the description of the simplified LS model which only contains the interface transportation. Secondly, the theoretical model of LS is a purely buoyancy-driven model which doesnt include any effect of dynamically-driven stratified turbulence. Without stratified turbulence, the unstably stratified boundary layer becomes necessary for the flux transport in their model. However, when the effect of stratified turbulence is properly taken into account in our model, the flux transport can be achieved solely by stratified turbulence (as in our simulation with $R_\rho = 5$, 8 and $R_\rho = \infty$). Therefore the staircase structure can stably exist in those systems even though they are predicted to be unstable by LSs theory.

SUMMARY AND CONCLUSIONS

In this paper, we have performed a series of DNS analyses of the continuously forced stratified turbulent system comprised of two different scalars stratified in the diffusive-convection configuration. We found that thermohaline layered structure forms spontaneously in the

simulations. We then considered three different aspects of this process to show that it is indeed well explained by the theory of MP21. First we showed that the controlled parameter Re_b in the layering simulations do satisfy the criterion derived by MP21. Secondly we have demonstrated that the key assumption of the Re_b instability theory of MP21, namely that the [28] parametrization scheme determines the vertical transports of the system, is indeed the case in the layer formation stage of our system. Third we have found good consistency between the exponential growing of the layering mode with the predicted growth-rate from the linear theory of MP21. These results strongly support the conclusion that the Re_b instability theory of MP21 is the correct explanation of thermohaline staircase formation in the diffusive convection regime that is characteristic of the Arctic Ocean.

The staircases formed in our DNS simulations were next examined and compared with the model proposed by LS. We explained how the vertical fluxes are kept balanced in our model despite the fact that the boundary layer structure that has been regarded as critical in stabilizing the interface structure is missing in our model. We have argued that the reason for the discrepancies between the classical model and our simulations is because they did not consider the stratified turbulence that may exist within their original model in the boundary layers and mixed layers.

There are several limitations of the numerical simulations that we have performed as basis for the discussion of the detailed staircase formation processing this paper. Firstly it should be kept in mind that all of the simulations have performed have assumed a Schmitt number Sc=70 which is an order of magnitude smaller than the typical value of Sc=700. This prevents us from directly comparing the values of fluxes obtained from our simulations with the empirical interface flux laws calibrated previously (e.g. [48], [52] [53]). Secondly we do not as yet know whether the steady staircase state we observed is in its equilibrium. It is possible that after a much longer integration time (and higher domains) the current stable stabilized staircases will continue to merge together. Observing such trends in DNSs requires a huge number of computational resources.

On the theoretical perspective, we have mentioned several times in the paper that the [28]'s parametrization of reaches its limit for describing small-scale dynamics of the system. Therefore, we believe that a properly captured multi-scale theory as that has been done in salt-fingering staircase ([16]) is the key for us to make further deep understanding for the diffusive-convection staircases.

Appendix A: Influences of resolution on the direct numerical simulations

As we have discussed in the main text, the long integration time needed for the system to develop into the staircase state exerts a strong constraint on the resolution available for our numerical simulations. In order to understand the influences of resolution in our numerical system, we performed two control experiments for simulation number 1 and number 2 with the same numerical settings except for a coarser resolution that has half the number of grid points in each of three spatial dimensions ($175 \times 175 \times 175$ grid points). In what follows, we will use low-res, mid-res and high-res to refer to the resolution of $175 \times 175 \times 175$ grids, $350 \times 350 \times 350$ grids and $700 \times 700 \times 700$ grids separately.

In Figure 11(a-c) we compare the evolution of vertical spectrum of salinity for the critical layering mode between low-res simulation and mid-res simulation (spectrum evolution of midres has been shown and discussed in the main text) for $R_\rho = 2$, 5 and 8 with $P = 0.01$. Although the systems take a different path and different time periods towards the equilibrium as we switched the resolution, the equilibrium states for the vertical structure they reach are almost identical. This can be seen in Figure 11(d-f), which shows the comparison of vertical profiles for temperature and salinity between low-res simulation and mid-res simulation in the equilibrium state. These vertical profiles show almost the same structure except for the fact that the interface gradients for low-res simulation are slightly smaller for $R_\rho = 2$. This suggests that the formation of the staircase state in our numerical system is a robust result instead of a numerical artifact.

Although the variation of resolution doesnt influence the final equilibrium staircase state of our numerical simulations, the vertical heat flux and salt flux in the equilibrium state are found to be sensitive to the resolutions. To see this, we evaluate the Nusselt numbers for heat and salt, which are the commonly used non-dimensional numbers that reflect the ratio of convective flux over diffusive flux defined as:

$$\begin{aligned} Nu_\Theta &= RePr\langle w'\Theta'\rangle \\ Nu_S &= ReSc\langle w'S'\rangle \end{aligned} \tag{24}$$

In Figure 12, we plot the variation of the Nusselt numbers as a function of three different resolutions applied in the equilibrium layered stage in our simulations with $R_\rho = 2$, 5 and 8 separately. Both Nu_Θ and Nu_S increases with the increased resolution for all our simulations, especially for the increase of Nu_S from low-res simulation to mid-res. The fact

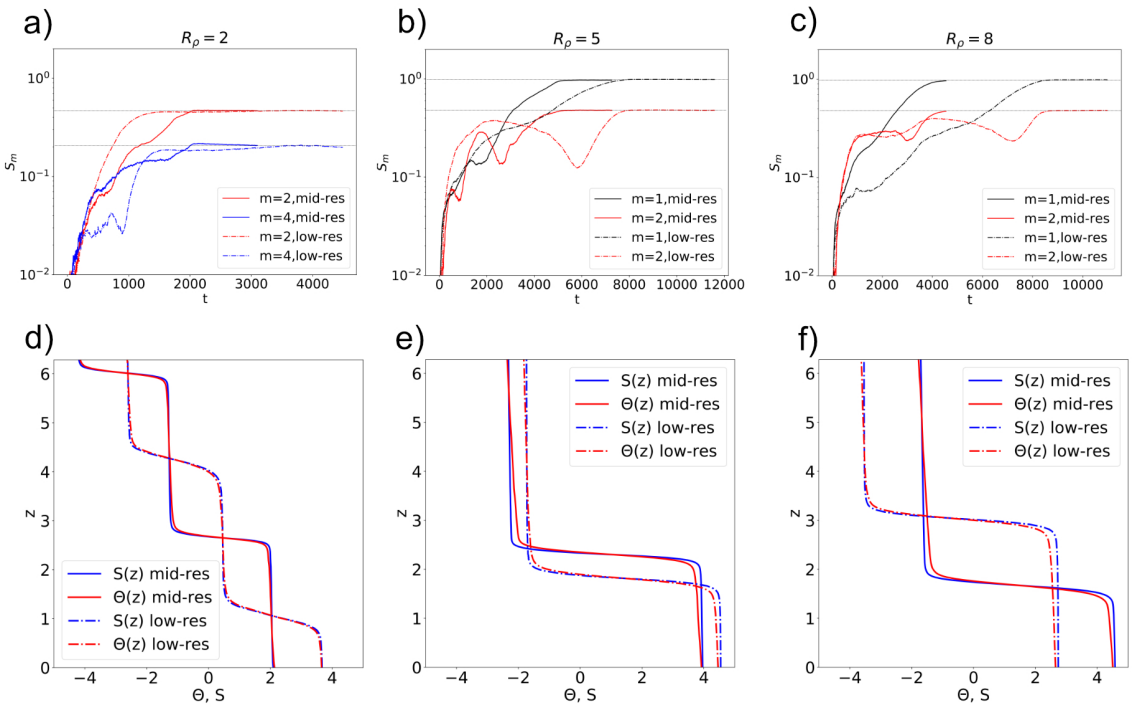

FIG. 11. (a-c): Comparision of vertical spectrum of salinity between low-res simulation and mid-res simulation for R_ρ=2 (a), R_ρ=5 (b) and R_ρ=8 (c) separately. (d-f) Comparison of vertical profiles of $\overline{\Theta}(z)$ and $\overline{S}(z)$ in the equilibrium staircase state between low-res simulation and mid-res simulation

that only mild increase of fluxes occur during the improvement of resolution from mid-res to high-res suggests that further increase of resolution will not bring significant variation to the equilibrium transport we have simulated. However, it still needs to be remembered that these values of fluxes we have obtained is under limited resolution and should be viewed with caution.

[1] Y. Ma and W. Peltier, Thermohaline staircase formation in the diffusive convection regime: a theory based upon stratified turbulence asymptotics, Journal of Fluid Mechanics **931** (2022).

[2] P. Linden and T. Shirtcliffe, The diffusive interface in double-diffusive convection, Journal of Fluid Mechanics **87**, 417 (1978).

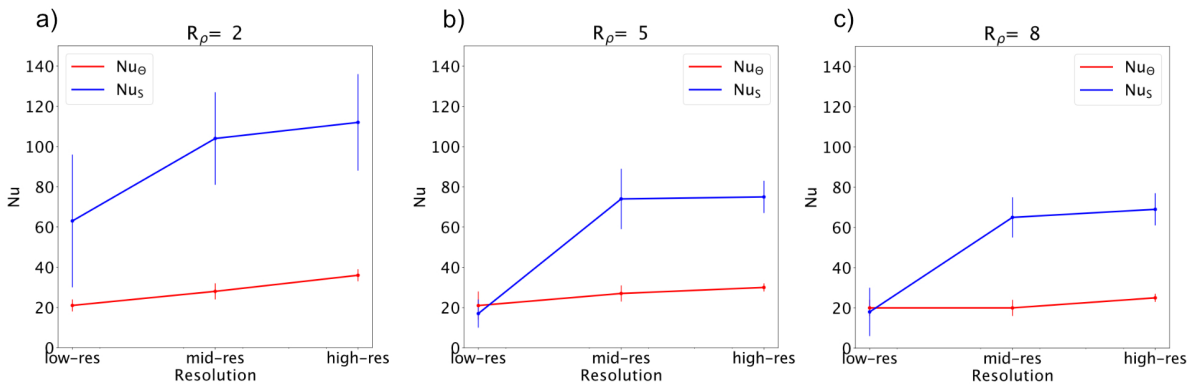

FIG. 12. (a-c): Comparison of Nusselt number for Temperature Nu_Θ and Salinity Nu_S in the equilibrium layered stage for $R_\rho = 2$ (a), $R_\rho = 5$ (b) and $R_\rho = 8$(c) separately. The error bars are based on 95% confidence interval.

[3] T. Radko, *Double-diffusive convection* (Cambridge University Press, 2013).

[4] R. Tait and M. Howe, Some observations of thermo-haline stratification in the deep ocean, in *Deep Sea Research and Oceanographic Abstracts*, Vol. 15 (Elsevier, 1968) pp. 275–280.

[5] V. T. Neal, S. Neshyba, and W. Denner, Thermal stratification in the arctic ocean, Science **166**, 373 (1969).

[6] T. Radko, A mechanism for layer formation in a double-diffusive fluid, Journal of Fluid Mechanics **497**, 365 (2003).

[7] M. E. Stern, T. Radko, and J. Simeonov, Salt fingers in an unbounded thermocline, Journal of marine research **59**, 355 (2001).

[8] A. Traxler, S. Stellmach, P. Garaud, T. Radko, and N. Brummell, Dynamics of fingering convection. part 1 small-scale fluxes and large-scale instabilities, Journal of fluid mechanics **677**, 530 (2011).

[9] T. Radko and D. P. Smith, Equilibrium transport in double-diffusive convection, Journal of fluid mechanics **692**, 5 (2012).

[10] Y. Ma and W. Peltier, Parametrization of irreversible diapycnal diffusivity in salt-fingering turbulence using dns, Journal of Fluid Mechanics **911** (2021).

[11] L. St. Laurent and R. W. Schmitt, The contribution of salt fingers to vertical mixing in the north atlantic tracer release experiment, Journal of Physical Oceanography **29**, 1404 (1999).

[12] R. W. Schmitt Jr, The growth rate of super-critical salt fingers, Deep Sea Research Part A. Oceanographic Research Papers **26**, 23 (1979).

[13] S. Stellmach, A. Traxler, P. Garaud, N. Brummell, and T. Radko, Dynamics of fingering convection. part 2 the formation of thermohaline staircases, Journal of Fluid Mechanics **677**, 554 (2011).

[14] T. Radko, A. Bulters, J. Flanagan, and J.-M. Campin, Double-diffusive recipes. part i: Large-scale dynamics of thermohaline staircases, Journal of physical oceanography **44**, 1269 (2014).

[15] T. Radko, What determines the thickness of layers in a thermohaline staircase?, Journal of Fluid Mechanics **523**, 79 (2005).

[16] T. Radko, Thermohaline layering on the microscale, Journal of Fluid Mechanics **862**, 672 (2019).

[17] Y. Ma and W. Peltier, Gamma instability in an inhomogeneous environment and salt-fingering staircase trapping: Determining the step size, Physical Review Fluids **6**, 033903 (2021).

[18] R. W. Schmitt, Double diffusion in oceanography, Annual Review of Fluid Mechanics **26**, 255 (1994).

[19] M.-L. Timmermans, J. Toole, R. Krishfield, and P. Winsor, Ice-tethered profiler observations of the double-diffusive staircase in the canada basin thermocline, Journal of Geophysical Research: Oceans **113** (2008).

[20] N. Shibley, M.-L. Timmermans, J. Carpenter, and J. Toole, Spatial variability of the arctic ocean's double-diffusive staircase, Journal of Geophysical Research: Oceans **122**, 980 (2017).

[21] T. Radko, Thermohaline layering in dynamically and diffusively stable shear flows, Journal of Fluid Mechanics **805**, 147 (2016).

[22] J. M. Brown and T. Radko, Initiation of diffusive layering by time-dependent shear, Journal of Fluid Mechanics **858**, 588 (2019).

[23] T. Radko, Thermohaline-shear instability, Geophysical Research Letters **46**, 822 (2019).

[24] W. J. Merryfield, Origin of thermohaline staircases, Journal of Physical Oceanography **30**, 1046 (2000).

[25] Y. Bebieva and M.-L. Timmermans, The relationship between double-diffusive intrusions and staircases in the arctic ocean, Journal of Physical Oceanography **47**, 867 (2017).

[26] O. Phillips, Turbulence in a strongly stratified fluidis it unstable?, in *Deep Sea Research and Oceanographic Abstracts*, Vol. 19 (Elsevier, 1972) pp. 79–81.

[27] J. Taylor and Q. Zhou, A multi-parameter criterion for layer formation in a stratified shear flow using sorted buoyancy coordinates, Journal of Fluid Mechanics **823** (2017).

[28] D. Bouffard and L. Boegman, A diapycnal diffusivity model for stratified environmental flows, Dynamics of Atmospheres and Oceans **61**, 14 (2013).

[29] H. Dosser, M. Chanona, S. Waterman, N. Shibley, and M.-L. Timmermans, Changes in internal wave-driven mixing across the arctic ocean: Finescale estimates from an 18-year pan-arctic record, Geophysical Research Letters **48**, e2020GL091747 (2021).

[30] J. Carpenter, T. Sommer, and A. Wüest, Simulations of a double-diffusive interface in the diffusive convection regime, Journal of Fluid Mechanics **711**, 411 (2012).

[31] N. Shibley and M.-L. Timmermans, The formation of double-diffusive layers in a weakly turbulent environment, Journal of Geophysical Research: Oceans **124**, 1445 (2019).

[32] D. Kelley, H. Fernando, A. Gargett, J. Tanny, and E. Özsoy, The diffusive regime of double-diffusive convection, Progress in Oceanography **56**, 461 (2003).

[33] J. Turner, A physical interpretation of the observations of hot brine layers in the red sea, in *Hot brines and recent heavy metal deposits in the Red Sea* (Springer, 1969) pp. 164–173.

[34] A. Boldrin and S. Rabitti, Hydrography of the brines in the bannock and tyro anoxic basins (eastern mediterranean), Marine chemistry **31**, 21 (1990).

[35] M. L. Waite and P. Bartello, Stratified turbulence dominated by vortical motion, Journal of Fluid Mechanics **517**, 281 (2004).

[36] G. Brethouwer, P. Billant, E. Lindborg, and J.-M. Chomaz, Scaling analysis and simulation of strongly stratified turbulent flows, Journal of Fluid Mechanics **585**, 343 (2007).

[37] A. Maffioli, G. Brethouwer, and E. Lindborg, Mixing efficiency in stratified turbulence, Journal of Fluid Mechanics **794** (2016).

[38] C. J. Howland, J. R. Taylor, and C. Caulfield, Mixing in forced stratified turbulence and its dependence on large-scale forcing, Journal of Fluid Mechanics **898** (2020).

[39] P. F. Fischer, J. W. Kruse, Lottes, and S. Kerkemeier, Nek5000 webpage http://nek5000.mcs.anl.gov. (2008).

[40] P. F. Fischer, An overlapping schwarz method for spectral element solution of the incompressible navier–stokes equations, Journal of Computational Physics **133**, 84 (1997).

[41] P. Fischer and J. Mullen, Filter-based stabilization of spectral element methods, Comptes Rendus de l'Académie des Sciences-Series I-Mathematics **332**, 265 (2001).

[42] R. Furue, Energy transfer within the small-scale oceanic internal wave spectrum, Journal of physical oceanography **33**, 267 (2003).

[43] A. Nelson, B. Arbic, D. Menemenlis, W. Peltier, M. Alford, N. Grisouard, and J. Klymak, Improved internal wave spectral continuum in a regional ocean model, Journal of Geophysical Research: Oceans **125**, e2019JC015974 (2020).

[44] Y. Pan, B. K. Arbic, A. D. Nelson, D. Menemenlis, W. Peltier, W. Xu, and Y. Li, Numerical investigation of mechanisms underlying oceanic internal gravity wave power-law spectra, Journal of Physical Oceanography **50**, 2713 (2020).

[45] P. Garaud, Double-diffusive convection at low prandtl number, Annual Review of Fluid Mechanics **50**, 275 (2018).

[46] L. Padman and T. M. Dillon, Thermal microstructure and internal waves in the canada basin diffusive staircase, Deep Sea Research Part A. Oceanographic Research Papers **36**, 531 (1989).

[47] Y. Yang, R. Verzicco, D. Lohse, and C. Caulfield, Layering and vertical transport in sheared double-diffusive convection in the diffusive regime, Journal of Fluid Mechanics **933** (2022).

[48] D. E. Kelley, Fluxes through diffusive staircases: A new formulation, Journal of Geophysical Research: Oceans **95**, 3365 (1990).

[49] T. Newell, Characteristics of a double-diffusive interface at high density stability ratios, Journal of Fluid Mechanics **149**, 385 (1984).

[50] M. G. Worster, Time-dependent fluxes across double-diffusive interfaces, Journal of Fluid Mechanics **505**, 287 (2004).

[51] M. E. Stern, Inequalities and variational principles in double-diffusive turbulence, Journal of Fluid Mechanics **114**, 105 (1982).

[52] G. O. Marmorino and D. R. Caldwell, Heat and salt transport through a diffusive thermohaline interface, in *Deep Sea Research and Oceanographic Abstracts*, Vol. 23 (Elsevier, 1976) pp. 59–67.

[53] W. G. Large, J. C. McWilliams, and S. C. Doney, Oceanic vertical mixing: A review and a model with a nonlocal boundary layer parameterization, Reviews of geophysics **32**, 363 (1994).